

SMR/1328/2

School on the Physics of Equatorial Atmosphere
(24 September - 5 October 2001)

Observational Techniques

R. A. Vincent
(University of Adelaide)

1 Introduction

Improvements in our understanding of atmospheric processes has gone hand-in-hand with the development and application of new techniques for observing the atmosphere. There has been rapid development in the past few decades as new methods for sounding the atmosphere and ionosphere have become available. Techniques range from highly detailed “single-shot” observations from rocket- and balloon-borne instruments to more continuous observations made with ground-based instruments using the radiowave and optical spectrum. Recently, satellite observations have begun to play an important role in providing a global perspective.

It should be recognized that each technique has its own advantages and disadvantages for sounding the atmosphere and it is now increasingly common to “cluster” different instruments to make use of the best attributes of each. The following discussion is meant to serve as an introduction to the more commonly used techniques; it is not meant to be exhaustive.

2 Radiosonde Observations

A radiosonde is a balloon-borne package that makes observations as a function of height of temperature, humidity, and pressure. Radiosondes released daily by weather services around the world provide the primary information for studying the thermal and dynamical state of the atmosphere up to heights near 30 km.

The sonde, which is approximately the size of a shoebox, is suspended some distance below the balloon to reduce the effects of the wake as the balloon ascends. Using an onboard radio transmitter the information is telemetered regularly back to a ground receiving station. The rate at which data are received depends on the system used, but typically data are acquired at 10-sec intervals. Balloons ascend at about 5 ms^{-1} so the equivalent height resolution is about 50 m. However, data may not be finally reported and archived at this rate, and information at ‘significant levels’ only may actu-

ally be saved, which reduces the effective height resolution to $\sim 0.5\text{-}1$ km.

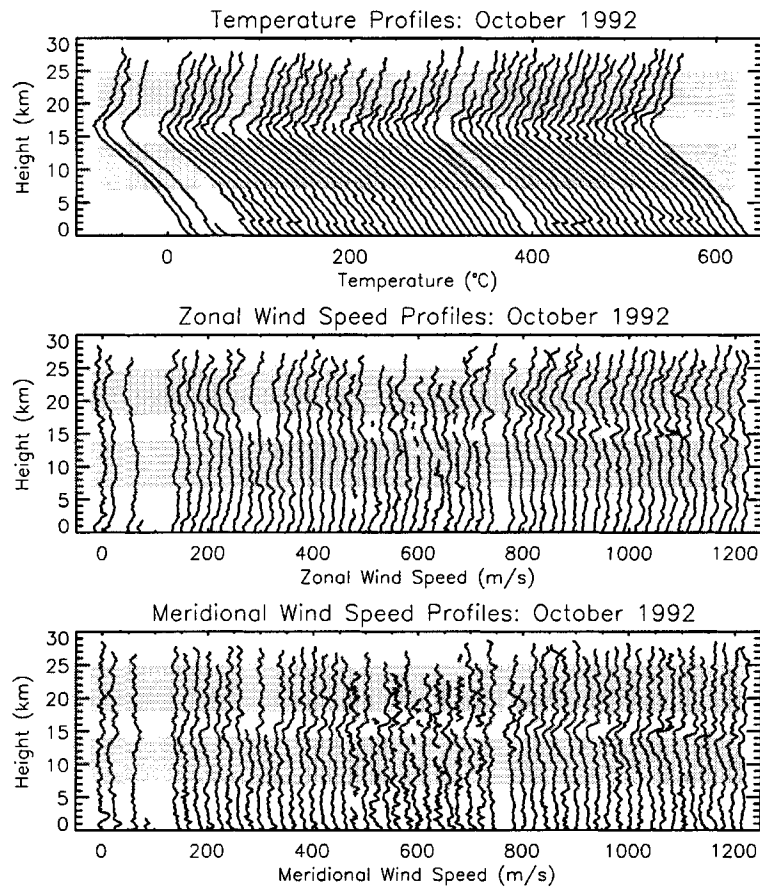


Figure 1: A sequence of radiosonde observations from Cocos Islands (12°S , 97°E)

The type of devices used to measure temperature and humidity depend on the manufacturer. For example, the widely used Vaisala sondes use a capacitive bead to measure temperature, with an accuracy of $0.2\text{-}0.3^{\circ}\text{C}$, and a thin film capacitor to measure humidity. Some stations also have the capability of measuring winds in the upper atmosphere if the position of the balloon is known as it ascends. One way is to use a ground-based radar to track the sonde. Alternatively, the sondes themselves carry a radio receiver capable of receiving signals from various navigation systems, such as Loran or

GPS, and transmitting their position to the ground station, which computes the wind speed and direction.

Weather agencies make synoptic observations twice a day at 0000 UTC and 1200 UTC from a network of stations spread across the globe. The actual height reached by a balloon before it bursts depends on such factors as the quality of the balloon and meteorological factors such as icing. Figure 2 shows a sequence of synoptic soundings made from the Cocos Island (12°S, 97°E) and illustrates some of the features of the tropical troposphere and lower stratosphere, including the cold and high tropopause at ~ 17 km. It shows that the upper level of most soundings is between 25 and 30 km, but that some balloons burst at much lower heights. Small wave-like features evident in the soundings, especially in the stratosphere, are interpreted as being due to atmospheric waves and radiosonde measurements have proved to be an important source of information on waves in the tropical lower atmosphere.

3 Radars

Ground-based radars (*R*Adio *D*etection and *R*Anging) enable atmospheric dynamics to be studied with a time resolutions as short as a few minutes. The most powerful systems can obtain information from near the ground to heights near 100 km, albeit with a 'gap' between 25 and 60 km. In principle radars can measure the three-dimensional wind field and other important quantities, such as turbulence parameters. They are an important source of information on atmospheric waves, such as gravity waves and tides.

There are many types of radar, each with their own particular characteristics. Here we concentrate on describing the types most commonly used for studies of the atmosphere from the ground up to heights near 100 km, with an emphasis on radars used to study the middle atmosphere. This height range includes the lower ionosphere, which extends upward from about 50 km during the day and from about 80 km at night. Table 1 shows the main radar types, together with typical frequency range of operation and

their nominal height coverage. The frequency ranges shown are only approximate, but cover the majority of systems. In the table MST stands for *Mesosphere-Stratosphere-Troposphere*. Less powerful radars of this type are called *Stratosphere-Troposphere (ST)* radars.

Table 1: Atmospheric radars

Type	Frequency (MHz)	Height Coverage (km)
Medium Frequency (MF)	2-3	60-100 (day) 80-100 (night)
Meteor wind radar (MWR)	30-50	80-105
MST	50	2-25 50-100 (day)
Incoherent Scatter (ISR)	430	60-100 (day)

The elements of a typical radar are shown in schematic form in Figure 2. Basically, a radar consists of a master oscillator/synthesiser to generate the frequency of the transmitted radiowave and other reference frequencies, a power amplifier for the transmitter, a transmitting antenna, one or more receiving antennas to collect the backscattered signals, one or more receiver to amplify the signals and a data acquisition system to digitise, integrate and store the signals for further computer manipulation. Radars are fully phase coherent so both phase and amplitude information is acquired. Most systems now have computing systems (often PCs) to analyse and present the data in almost real time. The majority of radars use co-located transmitting and receiving antennas. Many different antenna configurations are possible.

A single antenna can be used for both transmission and reception using a transmit/receive (T/R) switch, or the sub-modules of the transmitting antenna might be used, or separate transmitting and receiving antennas are used in some systems, in which case T/R switches are not required.

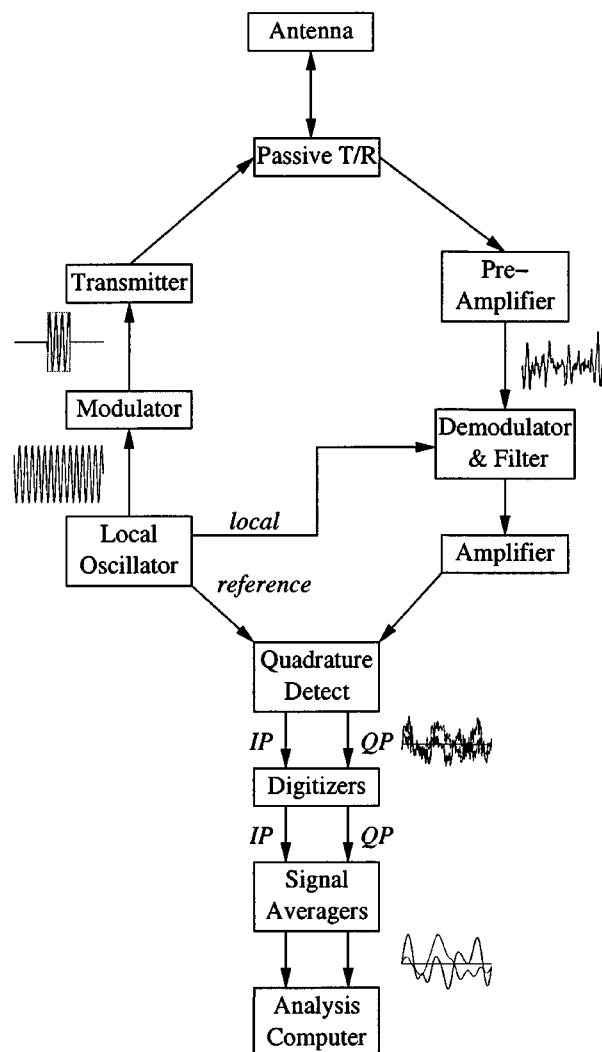


Figure 2: A radar in schematic form together with signal waveforms (after Tsuda, 1989)

Almost all atmospheric radars operate in pulsed mode so that the overall time of flight of a pulse determines the distance or range to a given echoing region (Figure 3). Pulses of duration Δt_{T_x} are transmitted at an interpulse

fluctuations, and dominates in the middle atmosphere. In the lower ionosphere (*D*-region), fluctuations in ionization determine the refractive index. The relative contribution of these three terms is illustrated in Figure 4 for a radar operating near 50 MHz.

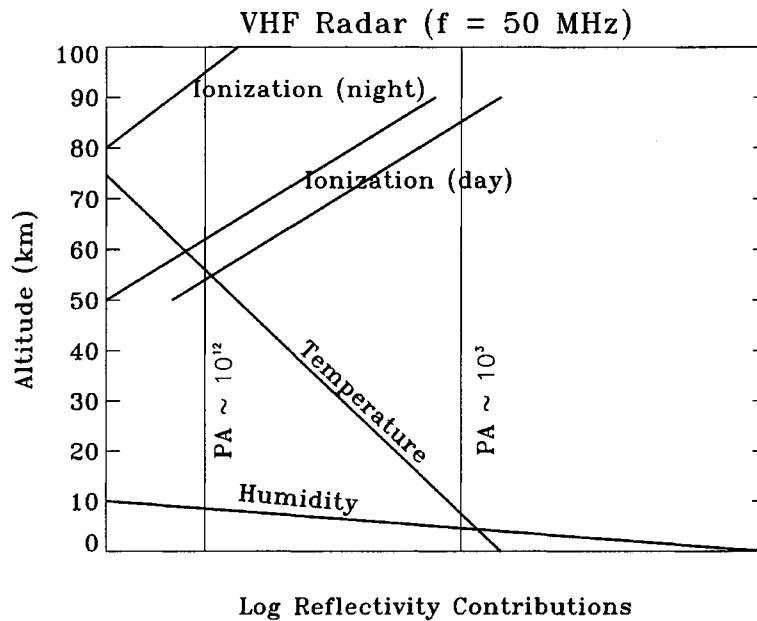


Figure 4: Altitude variation of relative refractivity contributions for VHF radars (after Röttger, 1984).

The actual received power and hence height coverage of a radar, depends on a number of factors. These include instrumental factors, such as the transmitter power and size of the antennas, and on atmospheric factors, such as the strength of turbulence. Two limiting processes may be considered for echoes received from a range R using a pulse length of ΔR . First, in the situation known as volume scatter, isotropic scatterers fill the volume defined by the radar beam and the pulse length the received power is given by the radar equation:

$$P_r = \frac{\pi P A \alpha \Delta R}{4\pi R^2} \eta \tag{2}$$

where P is the mean transmitted power, A is the effective antenna area, α is the overall efficiency of the radar, and η is the volume reflectivity. Sometimes,

however, echoes come from a sharply bounded discontinuity in refractive index (“Fresnel irregularity”), in which case the radar equation is:

$$P_r = \frac{PA^2}{4\lambda^2 R^2} |\rho|^2 \quad (3)$$

with λ as the radar wavelength and ρ is the amplitude reflection coefficient (Gage and Balsley, 1980). Partial reflections from horizontally stratified irregularities will be most important when the radar beam is pointing vertically. In between the extreme situations described by (2) and (3) different scattering/reflecting mechanisms can occur. Surprisingly, there is still much that we do not know about the mechanisms that give rise to the irregularities that cause radar scatter.

3.1 MST Radars

The common factor of PA or power-aperture product evident in (2) and (3) is often used as a figure of merit and used as a guide to the height coverage for a given radar. Two situations are shown in Figure 4 for a small system with a PA of $\sim 10^3 \text{ Wm}^2$ and a very large radar with a PA of $\sim 10^{12} \text{ Wm}^2$. The small system would be able to make measurements only up to heights near 10 km, while the very large system can observe throughout much of the atmosphere. At present only the 50 MHz MST radar at Jicamarca, Peru, has this capability. However, it is important to realize that at any given moment the actual height coverage depends on the presence of suitable scattering irregularities, which means on the strength of, for example, turbulence which can be highly variable in both space and time. The pointing direction of the radar beam is also a factor. As the beam is steered away from the zenith the received power decreases since the effects of specular reflections becomes less important and isotropic scattering dominates.

Unlike weather radars, which use mechanically steered dish antennas, atmospheric radars use fixed arrays of smaller antennas. The beam is pointed in different directions by introducing suitable electronic phasing between rows of antennas. For a given pointing direction atmospheric motions induce Doppler

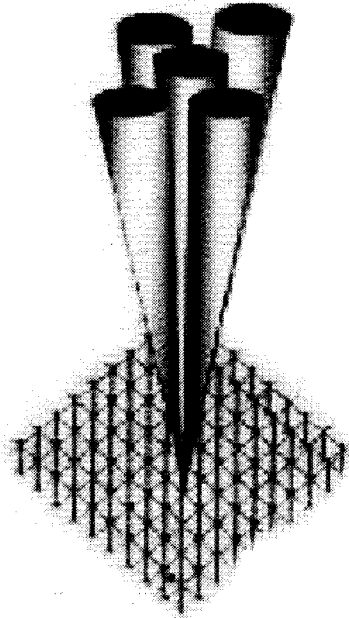


Figure 5: Conceptual VHF radar array and beams

shifts in the backscattered signals. For a radar with a sufficiently narrow beam pointing at an angle θ from the zenith at an azimuth of ϕ measured clockwise from North, the component of velocity along the beam is

$$v_r = u \sin\phi \sin\theta + v \cos\phi \sin\theta + w \cos\theta. \quad (4)$$

The use of at least three non-coplanar beams results in simultaneous equations for v_r , which can then be solved to determine the three-dimensional wind vector $\underline{V} = (u, v, w)$. An atmospheric radar using the Doppler technique uses a minimum of three beams to determine \underline{V} , but often 5 beams are used (Figure 5). Typical values for θ lie between 7 and 15° for routine observations at VHF. Since different volumes are being probed there is an assumption that the wind field is horizontally homogeneous.

The radar echoes can be analyzed in either the frequency or time domains. Analysis in the frequency domain requires an estimate of the power spectrum $S(f)$, an idealized example of which is shown in Figure 6. The atmospheric return has a Gaussian form with a Doppler shift of f_d and width Δf . P_N

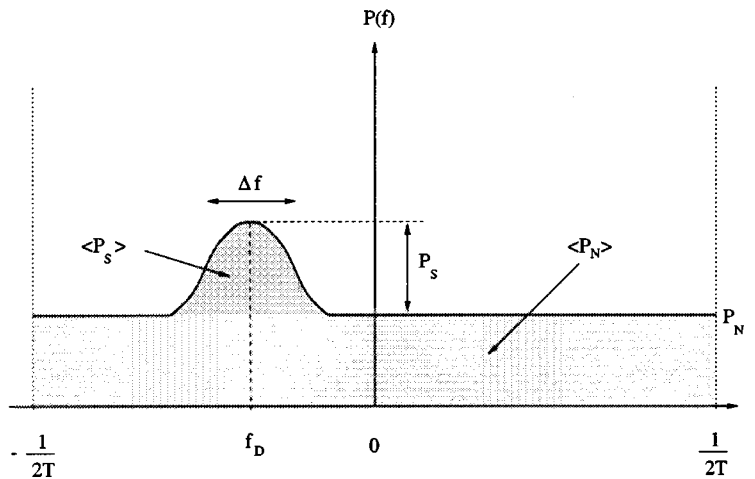


Figure 6: Idealized Doppler spectrum of atmospheric returns.

indicates the noise level. The radial velocity is related to f_D by

$$v_r = -\frac{4\pi}{\lambda} f_D \quad (5)$$

In the time domain the complex autocorrelation $\rho(\tau)$ is used, with the slope of the phase of ρ giving the Doppler shift.

Other important information about the atmosphere can be derived from either $S(f)$ or $\rho(\tau)$. The width of the spectrum Δf or equivalently the width of the autocorrelation function $\Delta\tau$ are partly determined by the strength of the random motions or turbulence. Extracting this information requires care, as the strength of the background wind and its shear with height also influence the spectral width (e.g. Hocking, 1985). Alternatively, the power returned by the scatterers can be used to find the rate of energy dissipation by turbulence.

Radars that use the Doppler technique to measure winds need narrow beams. Hence they require antennas with dimensions large compared with the radar wavelength. For MST-type radars operating at frequencies near 50 MHz (wavelength ~ 6 m) antenna arrays have dimensions larger than 50 m on a side. The Jicamarca radar has dimensions 150 m, producing a beam width of $< 1^\circ$.

3.2 MF Radars

Much of the discussion concerning MST and ST radars in the previous section also applies to radars operating in the MF band near 2 MHz. These radars detect echoes from fluctuations in electron density in the lower ionosphere. However, it should be recognized that birefringence in the ionosphere due to the presence of Earth's magnetic field becomes very important at these frequencies, which means that radiowaves can propagate in either of the ordinary or extraordinary characteristic modes. Equation (1) has to be modified to account for this effect.

The approximately f^{-2} factor in (1) means that ionospheric reflections are much easier to observe at MF than they are at VHF, especially at night. This means that it is less expensive to build an MF radar to study the dynamics of the mesosphere and lower thermosphere (Vincent, 1984). However, generating narrow beams at MF, where the wavelength is $\sim 100-150$ m, is difficult because of the large amounts of real estate required. Hence MF radars generally use another technique, the spaced-antenna method, to measure the wind velocity. One antenna is used for transmission and three non-collinear antennas are used for reception. The receiving antennas are usually arranged in the form of an equilateral triangle and all antennas are phased to point vertically. Radiowaves scattered from a given height form a diffraction pattern over the ground. If the atmosphere is in motion then the pattern also moves and the signal strengths at each receiving antenna show relative time displacements from which the velocity of the pattern and hence atmosphere can be calculated. While the Doppler and spaced-antenna techniques appear very different in practice they both make use of the Doppler shifts inherent in the backscattered signals and it is possible to derive the same information on winds and turbulence using both techniques (Briggs, 1980). From a practical point of view, each technique has its advantages and disadvantages.

3.3 Meteor Radars

Radiowaves from meteor wind radars are scattered from ionized trails in the upper mesosphere and lower thermosphere (MLT). The trails, formed as meteors ablate as they enter the atmosphere, usually last only a fraction of a second. The backscattered echoes suffer a Doppler shift as the trails are carried along by the neutral wind. Combining Doppler shift measurements of trails observed in different regions of the sky enables the wind velocity to be inferred. Locating the position of the trails requires either the use of narrow beam radars (often ST radars) or multiple receive antennas arranged as an interferometer. Usually it is assumed that the vertical wind component is small and can be neglected in comparison with the horizontal wind components. Observations of other atmospheric and astronomical interest can also be made. Diffusion causes the trails to expand, so measurements of the echo amplitude decay times allows diffusion coefficients and temperature to be inferred.

3.4 Incoherent Scatter Radars

Free electrons in the ionosphere act as Thompson scatterers when the plasma frequency is smaller than the radar frequency. As the electrons in a particular volume are in random motion the scattered waves add randomly. The ionosphere is a weak plasma, so the heavy ions constrain the scattering process and the high frequency of collisions between charged and neutral particles means that the scattering process is collision dominated. ISR have to be very powerful as the incoherent scatter cross-section is very small. For example the most powerful ISR, and the only one in tropical regions, the 430 MHz Arecibo (19°N) radar has peak power of a few MW. ISR can be used to study ion drift (neutral) velocities, temperatures, electron and neutral densities.

4 Lidars

Lidars (*L*Ight *D*etection and *R*Anging) are the optical equivalent of electromagnetic radars. Monochromatic optical pulses from a laser are backscattered from atmospheric molecules and detected as a function of range. At optical wavelengths the pulses can be very short, so the range resolution is usually very good (1.5 to 150 m). Various types of lidar operation are possible. The backscattered wavelength can either be the same as the transmitted wavelength (Rayleigh, Mie and resonant scattering) or at a higher wavelength (Raman and fluorescent scattering). Here we concentrate on Rayleigh and resonant scattering, which allow density and temperature measurements in the middle atmosphere.

A Rayleigh lidar consists of a laser transmitting vertically, a telescope to collect the returned light signals, which are then passed through a narrow band filter to reject unwanted stray light and focussed on a photomultiplier. Signals from the middle atmosphere are so weak that individual photons are counted. The problem of measuring signal amplitude as a function of height reduces to counting the number of pulses from the photomultiplier in a series of range gates (Kent and Wright, 1970).

Rayleigh scattering occurs when light waves are scattered by atmospheric molecules; Mie scattering occurs when atmospheric aerosols are involved. Above heights of ~ 30 to 35 km aerosol scattering is negligible compared to molecular scattering. In the regime where Rayleigh scattering dominates the lidar equation for a vertically pointing lidar is:

$$N(h) = \frac{N_o A \epsilon \mathcal{T}(0, h)}{4\pi h^2} n_o(h) \beta_R \Delta h \quad (6)$$

where N is the number of detected photons per laser pulse from a layer of thickness Δh and height h , N_o is the number of photons emitted for each laser pulse, A is the area of the collecting system (telescope), and ϵ is the overall efficiency of the optical system, including the quantum efficiency of the photomultiplier. The factors \mathcal{T} , n_o and β_R are, respectively, the total transmissivity of the atmosphere between the ground and height h , the number density of

atmospheric molecules, and the Rayleigh backscatter cross-section.

Equation (6) is inverted to find the atmospheric density ρ at height h

$$\rho(h) = N(h)K \frac{h^2}{\Delta h} \mathcal{T}^{-1} - n(h). \quad (7)$$

Here K is a normalization coefficient that depends on lidar specific factors N_o , A , and ϵ , and $n(h)$ is the number of photons due to electronic noise in the receiver and counting system and to sky background.

It is often difficult to calibrate lidar systems accurately so, in order to measure the absolute density profile, it is necessary to compare with an independent measurement at some convenient reference height. Usually, the calibration is made at heights near 30 km or above (where aerosol concentrations are small) using data acquired from a nearby radiosonde sounding.

Atmospheric temperature can also be obtained from the scattering profile. This is achieved through the use of the equation of state $p = R\rho T/M$ and hydrostatic equation $dp = -\rho g dz$, where p is pressure, M is the mean molecular mass, g the acceleration due to gravity and R is the universal gas constant. Eliminating p gives the temperature as a function of height

$$T(h) = \frac{\rho_1 T_1 + \frac{Mg}{R} \int_{h_1}^h \rho dh}{\rho(h)} \quad (8)$$

Note that an initial guess of the temperature T_1 at the top of the profile has to be made. This is usually done by using the appropriate value from a reference atmosphere such as the COSPAR international reference atmosphere (CIRA, 1986). As the integration proceeds downward any error due to incorrect choice of T_1 reduces out rapidly, so the actual value becomes of little consequence.

Resonant scattering occurs when the wavelength of light is close to that of an absorption line. A photon is absorbed and reemitted at the same wavelength if the life time of the excited state is short. Resonant scattering from sodium atoms in the 80-110 height region is an example where this processes is very useful for atmospheric studies. Although the abundance of Na atoms is small compared with the neutral atmospheric abundances the backscatter

cross-section is some 10^{14} times larger than for an atmospheric molecule. A Na lidar with only modest power-aperture product can be used. Figure 7

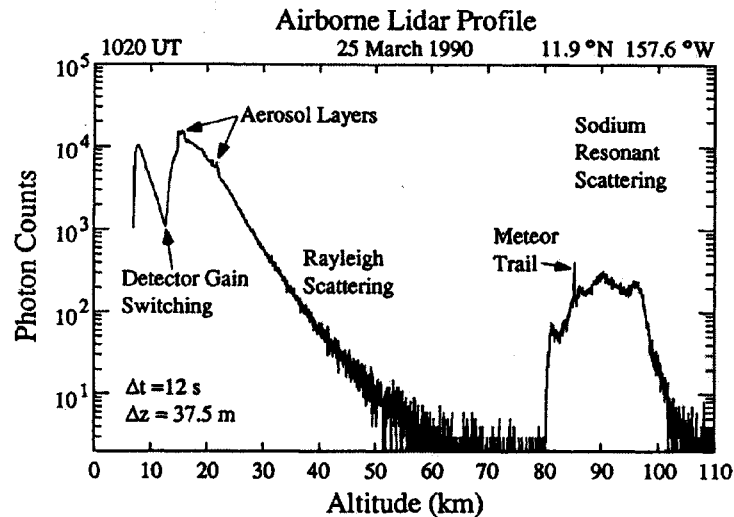


Figure 7: Lidar photon count profile from a Na/Rayleigh lidar mounted on an aircraft.

shows lidar observations of both Rayleigh and Na lidar measurements taken from systems mounted on an aircraft during the ALOHA-90 campaign to study low-latitude atmospheric processes and aeronomy; the campaign is described in a special section of the July 1991 edition of Geophysical Research Letters (GRL). A later campaign (ALOHA-93) is highlighted in the October 15, 1995 edition of GRL. The papers in these issues provide a good introduction to the diversity of ground and airborne techniques for studying the MLT.

In an important development She et al (1990) extended Na lidar studies to include temperatures in the mesopause region. Using a two-frequency narrowband lidar system they measured laser-induced fluorescence at two frequencies in the D_2 spectrum that are sensitive to temperature changes. One frequency is at the peak of the Na D_{2a} line and the other is at the crossover between the D_2 lines. This technique is becoming more widely used. Simultaneous observations of temperatures made with both the Rayleigh and

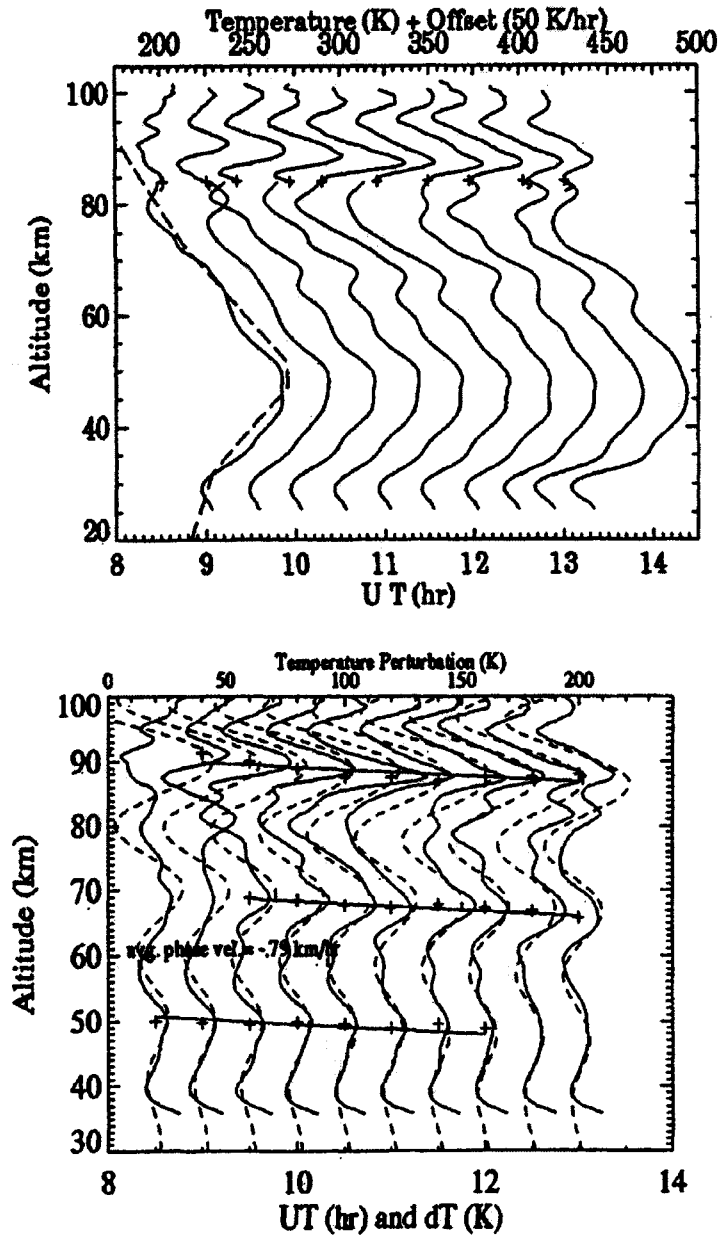


Figure 8: Composite temperature lidar profiles at 30-min intervals formed from Rayleigh and Na temperature measurements during ALOHA-93 (Top). Temperature perturbation profiles (Bottom).

Na lidar techniques are shown in Figure 8. Taken during the ALOHA-93 campaign in Maui, Hawaii, they show strong perturbations that may be due

to tides and/or gravity waves or to gravity wave-tidal interactions (Dao et al., 1995).

5 Rocket Observations

Rocket observations provided some of the first information on the state of the middle atmosphere, especially at low latitudes. Although rocket measurements are now less routinely made they still have an important role for specialized in-situ measurements in the middle atmosphere and lower thermosphere of processes that cannot be made by remote sensing from either ground or space. The main techniques of concern here use payloads deployed from rockets just as they reach apogee, and then tracked as they fall.

A rocketsonde is an instrumented package, rather like a radiosonde, but suspended from a parachute. Temperature and pressure measurements made on the way down are telemetered back to a ground station. Tracking the position of the sonde with a high precision radar enables the winds to be measured. The typical upper height limit of such a system is about 60 km. Rocketsondes formed the backbone of the meteorological rocket network (MRN) that made coordinated observations on a synoptic basis during the 1970s and 1980s. With a height resolution of ~ 500 m they provided an important source of information on winds and waves in the stratosphere, especially of gravity waves (e.g. Eckermann et al., 1995).

The falling sphere technique is an important method for measuring densities and temperatures. Using more powerful rockets than used for rocketsondes the sphere, which is made of metallic-coated Mylar, is carried to heights in excess of 100 km and inflated to a diameter of about 1 m after release. Initially, the sphere falls at supersonic speeds, but atmospheric drag slows the fall until the fall rate goes subsonic at heights near 70 km. The sphere collapses at heights near 30 km. If the acceleration of the sphere is measured by a high-precision tracking radar then atmospheric density can be determined with knowledge of the sphere's drag coefficient. Once the den-

sity profile is known then atmospheric temperature can be found from the equations of state and hydrostatics, in the same way as with a Rayleigh lidar (see equation 8). Tracking radar observations of the horizontal accelerations give the horizontal winds.

6 Satellite Techniques

6.1 UARS

Satellite measurements have played an increasingly important role in developing our understanding of middle atmosphere processes. In particular, instruments on the Upper Atmosphere Research Satellite (UARS) launched in September 1991 have been crucial for providing a global picture of prevailing winds, planetary-scale waves and tides and their effects on atmospheric composition. Nine instruments were deployed on UARS; details of the instruments and their capabilities can be found in the June 1993 edition of *Journal of Geophysical Research*. Of these instruments two were devoted specifically to direct measurements of the dynamics of the middle atmosphere and thermosphere.

The high resolution Doppler imager (HRDI) and wind imaging interferometer (WINDII) both measure Doppler shifts of airglow emission lines, although with rather different methods. Both are “limb viewing” instruments so that the weak emissions are observed against the cold background of space (Andrews et al., 1988). HRDI observes absorption and emission lines in the O_2 atmospheric band, scanning vertically to get a height profile. The instrument has a height coverage from about 60 to 115 km. Vector winds are obtained by observing the same atmospheric volume from nearly two orthogonal directions. WINDII works in a different way to HRDI. By observing a number of airglow lines it has a height coverage from about 80 km to 300 km. Both techniques require the inversion of limb-scanned data sets so they have similar sampling conditions. Their height resolution is ~ 2 km, but spatial averaging inherent in the limb-viewing geometry means that

their horizontal resolution is a few hundred kilometers.

6.2 GPS Occultation Techniques

Monitoring of signals from the constellation of global positioning system (GPS) satellites is becoming a powerful tool for atmospheric sounding. GPS satellites, which orbit the earth twice a day at an altitude of $\sim 20,200$ km, continuously transmit at frequencies of 1.2 GHz (L2) and 1.6 GHz (L1). As the signals propagate through the ionosphere and atmosphere they are refracted by vertical and horizontal variations in refractive index (equation 1). Ground-based observations of GPS signals can be used to measure both the total electron content (TEC) of the ionosphere and the integrated water vapour content of the atmosphere above the receiver, which has applications in improving weather forecasting. Businger et al (1996) and Ware et al (1996) provide an overview of both Earth- and satellite-based GPS monitoring of the atmosphere.

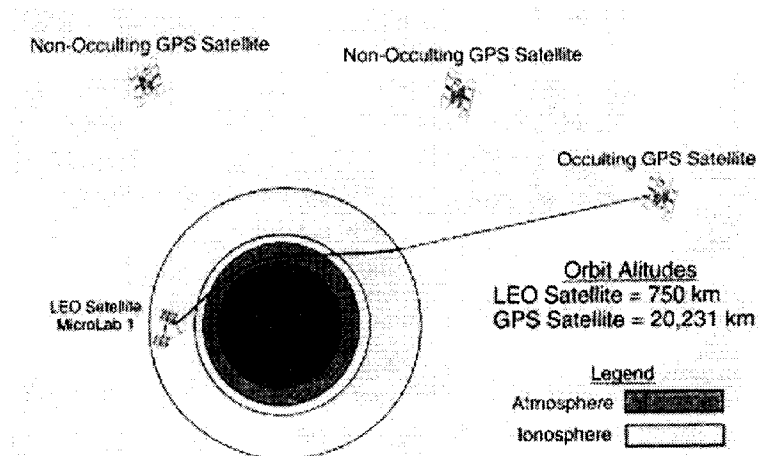


Figure 9: Schematic of a GPS/MET sounding of the Earth's atmosphere and ionosphere (after Ware et al., 1996)

The basic principles of spaced-based GPS techniques are illustrated in Figure 9, which shows a satellite in low Earth orbit (LEO) receiving signals

from an occulting GPS satellite. The signals are progressively delayed as they are refracted through increasingly longer paths through the ionosphere and neutral atmosphere. After accounting for the relative motion of the LEO and GPS satellites and drift of the clocks in the GPS transmitters it is possible to extract the delays caused by the refractive bending and propagation velocity changes caused by the ionosphere and atmosphere. The path delays are then converted to refractivity profiles, which can be sampled at a high rate down to almost the surface

As 1 shows the ionospheric component is dispersive (the L1 and L2 signals travel at different velocities) so the ionospheric delays can be removed. Equation (1), together with the hydrostatic equation, is then used to convert the refractivity profiles to profiles of pressure and temperature. Rather like the falling sphere and Rayleigh lidar techniques an initial temperature guess from a suitable climatology is used to initialize the inversion process at high altitudes. Any errors due to this guess are small at heights below ~ 50 km. Below about 5 to 10 km the moist term in (1) dominates and moisture profiles can be derived if p and T are known. More details can be found in Rocken et al. (1997)

The vertical resolution is limited to about 1.5 km by effects such as diffraction and horizontal atmospheric inhomogeneities, while the long slant path between the LEO and GPS satellites means that the horizontal resolution is ~ 300 km. The relatively small estimated temperature errors of 1°C in the 5 to 40 km height range and global coverage makes GPS measurements from space a very suitable technique for producing gravity wave climatologies, a potential that is now being realized (Tsuda et al., 2000).

7 Airglow Imager Observations

Weak optical emissions have been studied for many years to study the state of the upper atmosphere. It is not the purpose here to discuss the processes by which airglow is produced (they will be discussed in the second week

lectures), but rather to note that they provide a means by which waves and their effects can be directly visualized.

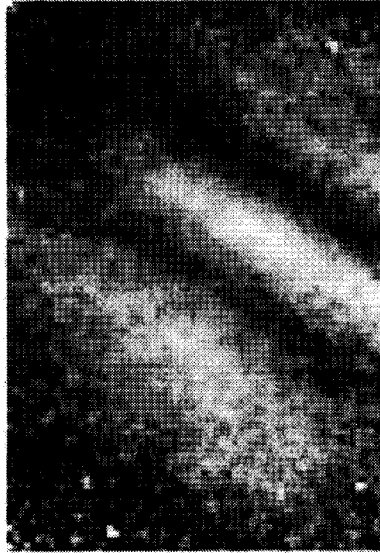


Figure 10: An image of OH airglow (843.0 nm) obtained on February 13, 2000 at the Buckland Park field station near Adelaide. The field of view is $50 \times 75^\circ$ (equivalent to $\sim 80 \times 135$ km), with north at the top and west to the right. The image exposure was for 1 minute and the brightest OH emission appears white (courtesy of J. H. Hecht).

Airglow imagers are essentially cameras which focus light onto a CCD array so that the output can be stored electronically. Narrow-band filters isolate particular emissions, so sequential changing of filters enables airglow from different height regions to be studied. For example, OH Meinel, O_2 atmospheric bands and 557.7 nm airglow emissions come from heights of about 87, 93 and 97 km. Comparing intensities from different lines in a give wavelength band also makes it possible to measure temperature.

An example of fluctuations in OH airglow intensity is given in Figure 10. The image, made from a 1 minute exposure, shows features with horizontal scales of about 40 km. Movies from sequential exposures allows the direction and speed of travel to be estimated, and if independent wind measurements from a radar, say, are available then the intrinsic wave properties can be

found. These observations were made with an imager that had a relatively narrow field of view, but some instruments provide images over almost the complete sky. Instruments with wide and narrow fields of view have their own advantages and disadvantages.

References

- [1] Andrews, D.G., J.R. Holton, and C.B. Leovy, *Middle Atmosphere Dynamics*, 489 pp., Academic, San Diego, Calif., 1987.
- [2] Briggs, B.H., Radar observations of atmospheric winds and turbulence: A comparison of techniques, *J. Atmos. Terr. Phys.*, *42*, 823-833, 1980.
- [3] Businger, S., and coauthors, The promise of GPS in atmospheric monitoring, *Bull. Amer. Meteor. Soc.*, *77*, 5-18, 1996.
- [4] Dao, P.D., R. Farley, X. Tao, and C.S. Gardner, Lidar observations of the temperature profile between 25 and 103 km: Evidence of strong tidal perturbation, *Geophys. Res. Lett.*, *22*, 2825-2828, 1995.
- [5] Eckermann, S.D., I. Hirota, and W.K. Hocking, Gravity wave and equatorial wave morphology of the stratosphere derived from long-term rocket soundings, *Q. J. R. Meteorol. Soc.*, *121*, 149-186, 1995.
- [6] Gage, K.S., and B.B. Balsley, On the scattering and reflection mechanisms contributing to clear air radar echoes from the troposphere, stratosphere and mesosphere, *Radio Sci.*, *15* 243-257, 1980.
- [7] Hocking, W.K., Measurements of turbulent energy dissipation rates in the middle atmosphere by radar techniques, *Radio Sci.*, *20*, 1403-1422, 1985.
- [8] Kent, G.S., and R.W.H. Wright, A review of laser radar measurements of atmospheric properties, *J. Atmos. Terr. Phys.*, *32*, 917-943, 1970.

- [9] Rocken, C., and coauthors, Analysis and validation of GPS/MET data in the neutral atmosphere, *J. Geophys. Res.*, *102*, 29,849-29,866, 1997.
- [10] Röttger, J., The MST radar technique, in *Handbook for Middle Atmosphere Program*, (ed. by R.A. Vincent), 187-232, SCOSTEP Secretariat, University of Illinois, 1984.
- [11] She, C.Y., H. Latifi, J.R. Yu, R.J. Alvarez, R.E. Bills, and C.S. Gardner, Two-frequency lidar technique for mesospheric Na temperature measurements, *Geophys. Res. Lett.*, *17*, 929-932, 1990.
- [12] Tsuda, T., Data acquisition and processing, in *Handbook for the Middle Atmosphere Program*, (ed. S. Fukao), 151-189, SCOSTEP Secretariat, University of Illinois, 1989.
- [13] Tsuda, T., M. Nishida, C. Rocken, and R. Ware, Global Morphology of Gravity Wave Activity in the Stratosphere Revealed by the GPS Occultation Data (GPS/MET), *J. Geophys. Res.*, *105*, 7257-7274, 2000.
- [14] Vincent, R.A., MF/HF radar measurements of the dynamics of the mesosphere region - A review, *J. Atmos. Terr. Phys.*, *46*, 961-974, 1984.
- [15] Ware, R., and coauthors, GPS sounding of the atmosphere from low Earth orbit: Preliminary results, *Bull. Amer. Meteor. Soc.*, *77*, 19-40, 1996.